Available online at www.sciencedirect.com
SCIENCE DIRECT®
Journal of Computational Physics 206 (2005) 597–623
JOURNAL OF COMPUTATIONAL PHYSICS
www.elsevier.com/locate/jcp

# Mach-uniformity through the coupled pressure and temperature correction algorithm

Krista Nerinckx *,[1], Jan Vierendeels, Erik Dick

*Department of Flow, Heat and Combustion Mechanics, Ghent University, Sint-Pietersnieuwstraat 41, B-9000 Ghent, Belgium*

Received 21 July 2004; received in revised form 23 December 2004; accepted 23 December 2004
Available online 8 February 2005

**Abstract**

We present a new type of algorithm: *the coupled pressure and temperature correction algorithm*. It is situated in between the fully coupled and the fully segregated approach, and is constructed such that Mach-uniform accuracy and efficiency are obtained. The essential idea is the separation of the convective and the acoustic/thermodynamic phenomena: a convective predictor is followed by an acoustic/thermodynamic corrector. For a general case, the corrector consists of a coupled solution of the energy and the continuity equations for both pressure and temperature corrections. For the special case of an adiabatic perfect gas flow, the algorithm reduces to a fully segregated method, with a pressure-correction equation based on the energy equation. Various test cases are considered, which confirm that Mach-uniformity is obtained.


*MSC:* 65N22; 76M12; 76N15; 76R10
*Keywords:* Mach-uniform; Segregated algorithm; Coupled algorithm; Pressure-correction; General fluid; Perfect gas; Adiabatic; Non-adiabatic

## 1. Introduction

Mach-uniform algorithms are an indispensable tool in numerous flow situations [1]. For years, the CFD-world has been searching for the ideal algorithm that can handle any level of the Mach number. With

* Corresponding author. Tel.: +32 9 264 33 00; fax: +32 9 264 35 86.
*E-mail addresses:* krista.nerinckx@ugent.be (K. Nerinckx), jan.vierendeels@ugent.be (J. Vierendeels), erik.dick@ugent.be (E. Dick).
[1] Research funded with a fellowship granted by the Flemish Institute for the Promotion of Scientific and Technological Research in the Industry (IWT).

0021-9991/$ - see front matter © 2005 Elsevier Inc. All rights reserved.
doi:10.1016/j.jcp.2004.12.019

preconditioning, the originally high speed density-based algorithms were extended toward the low Mach number regime [2,3]. The solution technique is then coupled and time accuracy can only be recovered through an expensive dual time stepping. As a segregated algorithm, the pressure-correction method is a well-established technique for incompressible flow [4]. Several attempts have been made to develop compressible pressure-correction methods [5–14]. Often, these algorithms are either not Mach-uniform or not applicable in general flow situations (for example, flows with heat transfer, a general fluid, etc.). In this paper, we aim to construct a collocated pressure-correction method that does have these features. A propagation analysis of the Euler and Navier–Stokes equations, valid for a general fluid, reveals how to reach Mach-uniformity. For a general flow, this leads to an algorithm that is situated in between the fully coupled and the fully segregated approach: the *coupled pressure and temperature correction algorithm*. When special cases are considered, like a constant density flow or the adiabatic flow of a perfect gas, the algorithm reduces to some well-known methods available in the literature.

## 2. Governing equations

For the sake of simplicity, we consider a one-dimensional non-viscous flow in a tube with a variable section $\hat{S}(x)$. The extension to two-dimensional viscous flow is straightforward. The governing Navier–Stokes equations are

$$\frac{\partial(\hat{\rho}\hat{S})}{\partial\hat{t}} + \frac{\partial(\hat{\rho}\hat{u}\hat{S})}{\partial\hat{x}} = 0, \tag{1}$$

$$\frac{\partial(\hat{\rho}\hat{u}\hat{S})}{\partial\hat{t}} + \frac{\partial(\hat{\rho}\hat{u}\hat{u}\hat{S})}{\partial\hat{x}} = -\hat{S}\frac{\partial\hat{p}}{\partial\hat{x}}, \tag{2}$$

$$\frac{\partial(\hat{\rho}\hat{E}\hat{S})}{\partial\hat{t}} + \frac{\partial(\hat{\rho}\hat{H}\hat{u}\hat{S})}{\partial\hat{x}} = -\frac{\partial(\hat{q}\hat{S})}{\partial\hat{x}}, \tag{3}$$

All dimensional quantities are denoted by a hat ($\hat{}$), e.g., $\hat{t}$, $\hat{\rho}$, $\hat{p}$, $\hat{u}$, $\hat{H}$, $\hat{E}$ and $\hat{x}$ denote, respectively, the time, density, pressure, velocity, total enthalpy, total energy and the spatial coordinate. Friction and external heat sources are neglected, but internal heat transfer due to conduction is taken into account. The heat flux $\hat{q}$ (W/m$^2$) is expressed by Fourier's law, $\hat{q} = -\hat{\kappa}(\partial\hat{T}/\partial\hat{x})$, with $\hat{\kappa}$ the heat conduction coefficient. The fluid is characterized by the equations of state,

$$\hat{\rho} = \hat{\rho}(\hat{p}, \hat{T}), \tag{4}$$

$$\hat{\rho}\hat{e} = \hat{\rho}\hat{e}(\hat{p}, \hat{T}), \tag{5}$$

with $e$ the specific internal energy.

The equations are non-dimensionalized by choosing three reference quantities, $\hat{p}_\mathrm{r}$, $\hat{T}_\mathrm{r}$ and $\hat{L}_\mathrm{r}$. Other reference quantities are calculated as

$$\hat{\rho}_\mathrm{r} = \hat{\rho}(\hat{p}_\mathrm{r}, \hat{T}_\mathrm{r}), \tag{6}$$

$$\hat{u}_\mathrm{r} = \sqrt{\frac{\hat{p}_\mathrm{r}}{\hat{\rho}_\mathrm{r}}}, \tag{7}$$

$$\hat{t}_\mathrm{r} = \hat{L}_\mathrm{r}/\hat{u}_\mathrm{r}, \tag{8}$$

$$\hat{e}_r = \hat{E}_r = \hat{H}_r = \hat{p}_r/\hat{\rho}_r. \tag{9}$$

The non-dimensional variables are defined as

$$p = \hat{p}/\hat{p}_r, \quad T = \hat{T}/\hat{T}_r, \ldots \tag{10}$$

The non-dimensional Navier–Stokes equations have the same structure as Eqs. (1)–(3), thus the latter are equally well valid for the non-dimensional variables. The RHS of the energy equation reads

$$\frac{\partial}{\partial x}\left(\kappa \frac{\partial T}{\partial x} S\right), \tag{11}$$

with

$$\kappa = \hat{\kappa}\frac{\hat{T}_r}{\hat{L}_r \hat{u}_r \hat{p}_r}, \tag{12}$$

the non-dimensional conduction coefficient. For a perfect gas, the non-dimensional equations of state read

$$\rho = p/T, \tag{13}$$

$$\rho e = \frac{1}{\gamma - 1} p, \tag{14}$$

with $\gamma$ the ratio of the specific heats.

## 3. Finite volume discretization

To discretize the equations, the flow domain is subdivided into a finite number of control volumes of length $\Delta x$. The variables are stored in the control volume center (collocated arrangement). The first node ($i = 1$) and the last node ($i = N$) coincide with the boundaries of the flow domain. A finite volume method is applied to discretize Eqs. (1)–(3). The time discretization is first order. The discretized version of the Navier–Stokes equations (1)–(3) reads

$$\rho_i^{n+1} - \rho_i^n + \frac{\tau}{S_i}\left[(\rho u S)_{i+\frac{1}{2}}^{n+1} - (\rho u S)_{i-\frac{1}{2}}^{n+1}\right] = 0, \tag{15}$$

$$(\rho u)_i^{n+1} - (\rho u)_i^n + \frac{\tau}{S_i}\left[(\rho u u S)_{i+\frac{1}{2}}^{n+1} - (\rho u u S)_{i-\frac{1}{2}}^{n+1}\right] = -\tau(p_{i+\frac{1}{2}}^{n+1} - p_{i-\frac{1}{2}}^{n+1}), \tag{16}$$

$$(\rho E)_i^{n+1} - (\rho E)_i^n + \frac{\tau}{S_i}\left[(\rho H u S)_{i+\frac{1}{2}}^{n+1} - (\rho H u S)_{i-\frac{1}{2}}^{n+1}\right] = -\frac{\tau}{S_i}\left[(qS)_{i+\frac{1}{2}}^{n+1} - (qS)_{i-\frac{1}{2}}^{n+1}\right], \tag{17}$$

where $n$ and $n + 1$ indicate the old and the new time level, respectively, $\tau = \Delta t/\Delta x$, and $\Delta t$ is the time step.

## 4. Mach-uniform accuracy

In a collocated arrangement, the problem of low Mach pressure–velocity decoupling is classically remedied by a Rhie–Chow interpolation for the cell face velocities [15].

However, in [16] we show that this causes the smearing of shocks in highly compressible flow. Therefore, it prevents reaching Mach-uniform accuracy. Thus, we will not use it in our algorithm. Instead, we work with the advection upwind splitting method (AUSM+) for the spatial discretization [17,18]. Though originally developed for density-based methods, the AUSM-flux fits perfectly in the context of pressure-based

methods because of the splitting into a convective and a pressure flux part. We apply a first-order upwind scheme for the transported quantities. The transporting velocity and the pressure at the cell faces are defined by Mach-dependent interpolations. At high Mach numbers, the AUSM-flux performs very well. At low Mach numbers special measures have to be taken with respect to the scaling and decoupling problem [19]. The bad scaling at low Mach numbers is remedied by introducing a preconditioned speed of sound and preconditioned Mach numbers. The low Mach pressure–velocity coupling is realized through the addition of a pressure-diffusion term to the cell face velocity. Under a compact notation, it reads

$$u_{i+\frac{1}{2}} = \tilde{u}_{i+\frac{1}{2}} - D_{i+\frac{1}{2}}(p_{i+1} - p_i), \tag{18}$$

with $\tilde{u}$ the cell face velocity defined by the AUSM+ interpolation. The expression for the coefficient $D$ can be found in [19]. However, we remark that it is not essential to follow this exact definition. A simplification is possible, as was done in [20].

We conclude that the AUSM+ flux realizes good accuracy, both in the low and high Mach number regime. Therefore, it allows us to reach Mach-uniform accuracy.

## 5. Mach-uniform efficiency

Mach-uniform efficiency implies a good convergence rate, whatever the Mach number is. Especially the low speed limit is critical, due to severe time step restrictions imposed by the stability of the scheme. These limits can be of an acoustic as well as of a diffusive nature.

The acoustic time step limit is expressed by the acoustic CFL-number,

$$\mathrm{CFL}_{u+c} = \frac{(u+c)\Delta t}{\Delta x} \leqslant \mathrm{CFL}^{\max}_{u+c}, \tag{19}$$

where $\mathrm{CFL}^{\max}_{u+c}$ is of the order unity. The highest allowable time step therefore is

$$\frac{\Delta t^{\max}}{\Delta x} = \frac{\mathrm{CFL}^{\max}_{u+c}}{u+c}. \tag{20}$$

The convective CFL-number is

$$\mathrm{CFL}_u = \frac{u\Delta t^{\max}}{\Delta x} = \frac{u}{u+c}\mathrm{CFL}^{\max}_{u+c} = \frac{1}{1+\frac{1}{M}}\mathrm{CFL}^{\max}_{u+c}, \tag{21}$$

which can be many orders lower than unity if the Mach number $M$ becomes small. Thus, a convective wave will need many time steps $\Delta t$ to travel one cell size $\Delta x$. This well-known stiffness problem destroys the convergence rate at low Mach numbers [21]. It therefore needs to be remedied in order to reach Mach-uniform efficiency.

Also a diffusive time step limit can have a devastating effect on the efficiency of the algorithm. This limit is expressed by the Von Neumann number,

$$Ne = \frac{\alpha\Delta t}{\Delta x^2} \leqslant \frac{1}{2}, \tag{22}$$

with $\alpha = \kappa/\rho c_p$ the thermal diffusivity. We get

$$\frac{\Delta t^{\max}}{\Delta x} = \frac{\frac{1}{2}\Delta x}{\alpha} \tag{23}$$

and

$$\mathrm{CFL}_u = \frac{1}{2}\frac{u\Delta x}{\alpha}. \tag{24}$$

If the diffusive phenomenon (conduction) dominates the convection, a low $CFL_u$-number will destroy the convergence rate once again. The same holds for the diffusive time step limit due to the viscous terms.

### 5.1. Removal of the acoustic time step limit

To remedy the stiffness problem, the acoustic CFL-limit has to be removed. [2] This can be obtained by treating implicitly the terms that carry acoustic information. In the following system of conservative Euler equations, we underlined those acoustic terms,

$$\underline{\frac{\partial \rho}{\partial t}} + \underline{\frac{\partial \rho u}{\partial x}} = 0, \tag{25}$$

$$\underline{\frac{\partial \rho u}{\partial t}} + \frac{\partial \rho uu}{\partial x} = -\underline{\frac{\partial p}{\partial x}}, \tag{26}$$

$$\underline{\frac{\partial \rho E}{\partial t}} + \underline{\frac{\partial \rho Hu}{\partial x}} = 0, \tag{27}$$

with

$$\underline{\rho E} = \underline{\rho e} + \tfrac{1}{2}\rho u^2, \tag{28}$$

$$\underline{\rho Hu} = \underline{(\rho e + p)u} + \tfrac{1}{2}\rho u^2 u. \tag{29}$$

We now explain how they were identified.

For this purpose, the Euler equations are transformed into a quasi-linear form. We expand the derivatives as

$$\underline{\frac{\partial \rho}{\partial t}} + u\frac{\partial \rho}{\partial x} + \rho\underline{\frac{\partial u}{\partial x}} = 0, \tag{30}$$

$$\rho\underline{\frac{\partial u}{\partial t}} + u\frac{\partial \rho}{\partial t} + \rho u\frac{\partial u}{\partial x} + u\frac{\partial \rho u}{\partial x} + \underline{\frac{\partial p}{\partial x}} = 0, \tag{31}$$

$$\underline{\frac{\partial \rho e}{\partial t}} + \frac{\partial}{\partial t}\left(\frac{1}{2}\rho u^2\right) + \underline{(\rho e + p)\frac{\partial u}{\partial x}} + u\frac{\partial \rho e}{\partial x} + u\frac{\partial p}{\partial x} + \frac{\partial}{\partial x}\left(\frac{1}{2}\rho u^2 u\right) = 0. \tag{32}$$

We replace Eq. (31) by (31) $- u *$ (25),

$$\rho\underline{\frac{\partial u}{\partial t}} + \rho u\frac{\partial u}{\partial x} + \underline{\frac{\partial p}{\partial x}} = 0 \tag{33}$$

and Eq. (32) by (32) $- u *$ (33) $- (1/2)u^2 *$ (30),

$$\underline{\frac{\partial \rho e}{\partial t}} + \underline{(\rho e + p)\frac{\partial u}{\partial x}} + u\frac{\partial \rho e}{\partial x} = 0. \tag{34}$$

Next, the system of equations (30), (33) and (34), is written in the primitive variables $p$, $u$, $T$,

[2] Another approach is to accept the limit, but to adapt the system such that the eigenvalues $u$, $u \pm c$ always remain of the same order. This is the philosophy of a time derivative preconditioning technique [2,3].

$$\rho_p\left(\frac{\partial p}{\partial t}+u\frac{\partial p}{\partial x}\right)+\rho_T\left(\frac{\partial T}{\partial t}+u\frac{\partial T}{\partial x}\right)+\rho\frac{\partial u}{\partial x}=0, \tag{35}$$

$$\rho\frac{\partial u}{\partial t}+\rho u\frac{\partial u}{\partial x}+\frac{\partial p}{\partial x}=0, \tag{36}$$

$$(\rho e)_p\left(\frac{\partial p}{\partial t}+u\frac{\partial p}{\partial x}\right)+(\rho e)_T\left(\frac{\partial T}{\partial t}+u\frac{\partial T}{\partial x}\right)+(\rho e+p)\frac{\partial u}{\partial x}=0. \tag{37}$$

Fluid properties were introduced, using the equations of state,

$$\rho=\rho(p,T) \tag{38}$$

$$\rho e=\rho e(p,T), \tag{39}$$

and

$$\rho_p=\left.\frac{\partial\rho}{\partial p}\right|_{T=\text{cst}},\qquad \rho_T=\left.\frac{\partial\rho}{\partial T}\right|_{p=\text{cst}}, \tag{40}$$

$$(\rho e)_p=\left.\frac{\partial(\rho e)}{\partial p}\right|_{T=\text{cst}},\qquad (\rho e)_T=\left.\frac{\partial(\rho e)}{\partial T}\right|_{p=\text{cst}}. \tag{41}$$

We now transform the system (35)–(37) into a quasi-linear system in $p$, $u$, $s$ ($s$ the entropy), from which the identification of acoustic terms will become clear. First, Eqs. (35) and (37) are combined to obtain an equation for pressure,

$$\left[\rho_p(\rho e)_T-(\rho e)_p\rho_T\right]\left(\frac{\partial p}{\partial t}+u\frac{\partial p}{\partial x}\right)+\left[\rho(\rho e)_T-(\rho e+p)\rho_T\right]\frac{\partial u}{\partial x}=0. \tag{42}$$

It can be written as

$$\frac{\partial p}{\partial t}+u\frac{\partial p}{\partial x}+\rho c^2\frac{\partial u}{\partial x}=0, \tag{43}$$

with

$$c^2=\left.\frac{\mathrm{d}p}{\mathrm{d}\rho}\right|_{s=\text{cst}} \tag{44}$$

the speed of sound. In Appendix A, we show that a general definition for the speed of sound is indeed given by

$$c^2=\frac{1}{\rho}\frac{(\rho e+p)\rho_T-\rho(\rho e)_T}{(\rho e)_p\rho_T-\rho_p(\rho e)_T}. \tag{45}$$

Next, Eqs. (35) and (37) are combined into an equation for the entropy $s$. With

$$T\,\mathrm{d}s=\mathrm{d}h-\frac{1}{\rho}\,\mathrm{d}p=\mathrm{d}e-\frac{p}{\rho^2}\,\mathrm{d}\rho=\mathrm{d}\left(\frac{\rho e}{\rho}\right)-\frac{p}{\rho^2}\,\mathrm{d}\rho, \tag{46}$$

we have,

$$\rho^2T\,\mathrm{d}s=\rho\,\mathrm{d}(\rho e)-(\rho e+p)\,\mathrm{d}\rho. \tag{47}$$

Thus, Eq. (37) $*\ \rho$ − Eq. (35) $*\ (\rho e+p)$ results in

$$\frac{\mathrm{D}s}{\mathrm{D}t} = 0, \tag{48}$$

which represents the convective transport of the entropy.

Eqs. (43), (36) and (48) form a quasi-linear system in $p$, $u$, $s$,

$$\frac{\mathrm{D}p}{\mathrm{D}t} + \underline{\rho c^2 \frac{\partial u}{\partial x}} = 0, \tag{49}$$

$$\frac{\mathrm{D}u}{\mathrm{D}t} + \underline{\frac{1}{\rho}\frac{\partial p}{\partial x}} = 0, \tag{50}$$

$$\frac{\mathrm{D}s}{\mathrm{D}t} = 0. \tag{51}$$

In system form it reads,

$$\frac{\mathrm{D}Q}{\mathrm{D}t} + A\frac{\partial Q}{\partial x} = 0, \tag{52}$$

with $Q = [p, u, s]^{\mathrm{T}}$, and

$$A = \begin{bmatrix} 0 & \rho c^2 & 0 \\ 1/\rho & 0 & 0 \\ 0 & 0 & 0 \end{bmatrix}. \tag{53}$$

Written in this form, the system matrix $A$ has eigenvalues $\pm c$, therefore representing the acoustic part of the system. It is the term $\rho c^2(\partial u/\partial x)$ from the pressure equation (49) and the term $(1/\rho)(\partial p/\partial x)$ from the velocity equation (50) which contribute to the acoustic part. This becomes even more clear when these two equations are combined to obtain an acoustic wave equation. Indeed, considering a pressure perturbation $p'$ above the convective flow and taking the time derivative of (49) yields

$$\frac{\mathrm{D}^2 p'}{\mathrm{D}t^2} + \rho c^2 \frac{\partial}{\partial x}\left(\frac{\mathrm{D}u'}{\mathrm{D}t}\right) = 0. \tag{54}$$

Combination with (50) results in the following acoustic wave equation:

$$\frac{\mathrm{D}^2 p'}{\mathrm{D}t^2} - c^2 \frac{\partial^2 p'}{\partial x^2} = 0, \tag{55}$$

for a pressure perturbation $p'$ at speed $c$.

In the system (49)–(51), the acoustic terms are underlined. To remove the acoustic CFL-limit, the derivatives in these terms will have to be treated implicitly. In the quasi-linear form of the equations, this is trivial. However, since we aim at an algorithm for all Mach numbers, including the transonic regime, the discretization has to be done in fully conservative form. Therefore, we return to the conservative set (25)–(27), and we identify where the acoustic terms appear in the latter equations. This is made clear by underlining the concerning terms in each step of the analysis performed. Remark that the underlined $\partial/\partial t$-terms in fact contribute to the acoustic as well as to the convective system. From the set (25)–(27), it is clear that the acoustic information is found in the mass flux of the continuity equation, the pressure gradient of the momentum equation, and the static enthalpy flux of the energy equation. These terms have to be treated implicitly in order to remove the acoustic CFL-limit. In the static enthalpy flux, only the velocity $u$ has to be treated implicitly, since only this variable appears under a derivative in the acoustic term. For the same reason, in the mass flux, only the velocity has to be treated implicitly.

### 5.2. Removal of the diffusive time step limit

When the Navier–Stokes equations are considered, viscous terms occur in the momentum and the energy equation, and conductive terms occur in the energy equation. To avoid diffusive time step limits, also these terms have to be treated implicitly.

## 6. Special cases

The analysis in the previous paragraph is valid for a general fluid. At this point, however, it is very instructive to consider some special cases.

### 6.1. Special case 1: constant density

If the density $\rho$ is considered as constant, the continuity equation (35) reduces to the kinematic constraint $(\partial u/\partial x) = 0$, and the energy equation (37) becomes a transport equation for the temperature. Therefore, the pressure and the velocity are determined by the continuity and momentum equation, while the temperature follows from the energy equation. This is the philosophy of a classical incompressible pressure-correction method, where the Poisson equation for the pressure corrections is derived from the continuity equation.

### 6.2. Special case 2: barotropic flow

In a barotropic flow, the density only depends on the pressure, $\rho = \rho(p)$. Since then $\rho_T = 0$, the temperature dependence disappears from the continuity equation (37). Like for the constant density flow, the pressure and the velocity are determined by the continuity and the momentum equation.

### 6.3. Special case 3: perfect gas

For a perfect gas, the equation of state (14) reads

$$\rho e = \frac{p}{\gamma - 1}, \tag{56}$$

so that $\rho e$ depends only on the pressure. Therefore, the temperature dependence now disappears from the energy equation (37). Thus, the most straightforward procedure is to determine the pressure and the velocity from the energy and momentum equation, and to use the continuity equation afterward to determine the temperature.

However, when heat conduction is present, conductive temperature terms appear in the energy equation, so that it is no longer an equation for pressure alone. Eqs. (35) (continuity) and (37) (energy minus kinetic energy) become for this case

$$\rho_p\left(\frac{\partial p}{\partial t} + u\frac{\partial p}{\partial x}\right) + \rho_T\left(\frac{\partial T}{\partial t} + u\frac{\partial T}{\partial x}\right) + \rho\frac{\partial u}{\partial x} = 0, \tag{57}$$

$$(\rho e)_p\left(\frac{\partial p}{\partial t} + u\frac{\partial p}{\partial x}\right) + (\rho e + p)\frac{\partial u}{\partial x} = -\frac{\partial q(T)}{\partial x}, \tag{58}$$

showing that the continuity and energy equation together determine both pressure and temperature.

## 7. Implementation: the coupled pressure and temperature correction algorithm

### 7.1. Convective step: predictor

The first step in the algorithm is a predictor step for density and momentum. In the discretized continuity and momentum equation, (15) and (16), the transport velocity and the pressure are put at a known iteration level $k$. We leave the possibility open to perform more than one iteration per time level, but in practice only one iteration step per time step was taken, so that $k \equiv n$. The values for density and momentum computed in that way are indicated with a superscript *, i.e.

$$\rho_i^* - \rho_i^n + \frac{\tau}{S_i}\left[\rho_i^* u_{i+\frac{1}{2}}^k S_{i+\frac{1}{2}} - \rho_{i-1}^* u_{i-\frac{1}{2}}^k S_{i-\frac{1}{2}}\right] = 0, \tag{59}$$

$$(\rho u)_i^* - (\rho u)_i^n + \frac{\tau}{S_i}\left[(\rho u)_i^* u_{i+\frac{1}{2}}^k S_{i+\frac{1}{2}} - (\rho u)_{i-1}^* u_{i-\frac{1}{2}}^k S_{i-\frac{1}{2}}\right] = -\tau(p_{i+\frac{1}{2}}^k - p_{i-\frac{1}{2}}^k). \tag{60}$$

From $\rho^*$, $(\rho u)^*$ and $p^k$, an intermediate state $*$ is determined. The predictor step takes place under a frozen pressure. It therefore can be considered as a convective step. In the predictor equations above, the transported quantities $\rho^*$ and $(\rho u)^*$ are treated in an implicit way. The predictor could be made fully explicit by writing the convective terms at the old time level $n$, but a convective CFL limit then has to be respected.

The reason why we do not determine $u^*$ directly from (60) using old values $\rho^k$, is the good representation of a contact discontinuity. Since then the pressure and the velocity have to remain constant at every moment, no pressure and velocity corrections may be generated. Consequently, the predictor should not disturb the velocity values $u$, as they cannot be corrected afterwards. Therefore, correct values for $\rho$ have to be used in the momentum equation, which explains the need for a convective step from the continuity equation.

### 7.2. Acoustic/thermodynamic step: corrector

Corrections with respect to the predictor values are defined,

$$p^{n+1} = p^k + p', \tag{61}$$

$$(\rho u)^{n+1} = (\rho u)^* + (\rho u)', \tag{62}$$

$$T^{n+1} = T^* + T'. \tag{63}$$

They are introduced into the discretized equations, namely in the terms at the new time level. Amongst them are the implicit diffusive and acoustic terms identified in Section 5.

#### 7.2.1. Momentum equation

We write the momentum predictor equation (60) as

$$\begin{aligned}(\rho u)_i^* - (\rho u)_i^n + \frac{\tau}{S_i}\left\{(\rho u)_i^*\left[\tilde{u}_{i+\frac{1}{2}}^k - D_{i+\frac{1}{2}}(p_{i+1}^k - p_i^k)\right]S_{i+\frac{1}{2}} - (\rho u)_{i-1}^*\left[\tilde{u}_{i-\frac{1}{2}}^k - D_{i-\frac{1}{2}}(p_i^k - p_{i-1}^k)\right]S_{i-\frac{1}{2}}\right\} \\ = -\tau\left\{p_{i+\frac{1}{2}}^k - p_{i-\frac{1}{2}}^k\right\},\end{aligned} \tag{64}$$

where the pressure diffusion term from (18) was written down.

In the final momentum equation, the pressure gradient is written at the new time level $n + 1$, as it was identified as an acoustic term. Also the pressure terms coming from the pressure stabilization are treated implicitly,

$$(\rho u)_i^{n+1} - (\rho u)_i^n + \frac{\tau}{S_i}\left\{(\rho u)_i^{n+1}\left[\tilde{u}_{i+\frac{1}{2}}^k - D_{i+\frac{1}{2}}(p_{i+1}^{n+1} - p_i^{n+1})\right]S_{i+\frac{1}{2}} - (\rho u)_{i-1}^{n+1}\left[\tilde{u}_{i-\frac{1}{2}}^k - D_{i-\frac{1}{2}}(p_i^{n+1} - p_{i-1}^{n+1})\right]S_{i-\frac{1}{2}}\right\}$$
$$= -\tau\left\{p_{i+\frac{1}{2}}^{n+1} - p_{i-\frac{1}{2}}^{n+1}\right\}. \tag{65}$$

Subtraction of (65) and (64) gives

$$(\rho u)_i' + \frac{\tau}{S_i}\left\{(\rho u)_i' u_{i+\frac{1}{2}}^k S_{i+\frac{1}{2}} - (\rho u)_{i-1}' u_{i-\frac{1}{2}}^k S_{i-\frac{1}{2}}\right\} + \frac{\tau}{S_i}\left\{-(\rho u)_i^* D_{i+\frac{1}{2}}(p_{i+1}' - p_i')S_{i+\frac{1}{2}} + (\rho u)_{i-1}^* D_{i-\frac{1}{2}}(p_i' - p_{i-1}')S_{i-\frac{1}{2}}\right\}$$
$$= -\tau\left\{p_{i+\frac{1}{2}}' - p_{i-\frac{1}{2}}'\right\}, \tag{66}$$

where products of corrections were neglected. To make a segregated solution procedure possible, we need to simplify Eq. (66) into an expression which contains only the momentum correction at the node $i$. Therefore, we cross out the momentum corrections coming from the convective terms. We remark that in fact there is no strict justification why it would be allowed to do such an approximation. Consequently, due to this segregation procedure, a certain degree of implicitness in the convective terms is lost. We get as an expression for $(\rho u)_i'$,

$$(\rho u)_i' = \frac{\tau}{S_i}\left\{(\rho u)_i^* D_{i+\frac{1}{2}}(p_{i+1}' - p_i')S_{i+\frac{1}{2}} - (\rho u)_{i-1}^* D_{i-\frac{1}{2}}(p_i' - p_{i-1}')S_{i-\frac{1}{2}}\right\} - \tau\left\{p_{i+\frac{1}{2}}' - p_{i-\frac{1}{2}}'\right\}. \tag{67}$$

The pressure corrections at the faces are expressed by means of the AUSM interpolation formula [17],

$$p_{i+\frac{1}{2}}' = P_5^+(M_i)p_i' + P_5^-(M_{i+1})p_{i+1}'. \tag{68}$$

From (67) the momentum corrections at the nodes can be calculated once the pressure corrections are known.

The momentum corrections at the faces are written as

$$(\rho u)_{i+\frac{1}{2}}' = (\rho\tilde{u})_{i+\frac{1}{2}}' - \rho_i^* D_{i+\frac{1}{2}}(p_{i+1}' - p_i'). \tag{69}$$

The correction $(\rho\tilde{u})_{i+\frac{1}{2}}'$ is expressed as an average of node values. Indeed, ignoring the pressure diffusion terms, (67) can be written as

$$(\rho u)_i' = -\tau\Delta x\left.\frac{\partial p'}{\partial x}\right|_i. \tag{70}$$

The same holds at node $i+1$. We determine $(\rho\tilde{u})_{i+\frac{1}{2}}$ as a contracted average,

$$(\rho\tilde{u})_{i+\frac{1}{2}}' = -\frac{1}{2}\left(\tau\Delta x\left.\frac{\partial p'}{\partial x}\right|_i + \tau\Delta x\left.\frac{\partial p'}{\partial x}\right|_{i+1}\right) \approx -\tau\Delta x\left.\frac{\partial p'}{\partial x}\right|_{i+\frac{1}{2}} \approx -\tau(p_{i+1}' - p_i'), \tag{71}$$

being inspired by the expressions on a staggered grid or by the classical Rhie–Chow interpolation [22]. Thus, the relation between momentum corrections at the faces and pressure corrections is obtained from (69) and (71),

$$(\rho u)_{i+\frac{1}{2}}' = -\left[\tau + \rho_i^* D_{i+\frac{1}{2}}\right](p_{i+1}' - p_i'). \tag{72}$$

*7.2.2. Continuity equation*

In the continuity equation (15), the density is expandeds

$$\rho_i^{n+1} = \rho_i^* + \rho_p^* p_i' + \rho_T^* T_i'. \tag{73}$$

The mass flux, which is an acoustic term (see Eq. (25)), is corrected as

$$(\rho u)_{i+\frac{1}{2}}^{n+1} = (\rho u)_{i+\frac{1}{2}}^{*} + (\rho u)_{i+\frac{1}{2}}', \tag{74}$$

and the correction is expressed by (72). The continuity equation thus becomes an equation for both pressure and temperature corrections,

$$A_{i,i-1}p_{i-1}' + A_{i,i}p_i' + A_{i,i+1}p_{i+1}' + \rho_T^* T_i' = SC_i, \tag{75}$$

with

$$A_{i,i-1} = -\tau\left(\tau + \rho_{i-1}^* D_{i-\frac{1}{2}}\right)\frac{S_{i-\frac{1}{2}}}{S_i}, \tag{76}$$

$$A_{i,i} = \rho_p^* + \tau\left(\tau + \rho_i^* D_{i+\frac{1}{2}}\right)\frac{S_{i+\frac{1}{2}}}{S_i} + \tau\left(\tau + \rho_{i-1}^* D_{i-\frac{1}{2}}\right)\frac{S_{i-\frac{1}{2}}}{S_i}, \tag{77}$$

$$A_{i,i+1} = -\tau\left(\tau + \rho_i^* D_{i+\frac{1}{2}}\right)\frac{S_{i+\frac{1}{2}}}{S_i}, \tag{78}$$

$$SC_i = \rho_i^n - \rho_i^* - \frac{\tau}{S_i}\left[(\rho u)_{i+\frac{1}{2}}^{*} S_{i+\frac{1}{2}} - (\rho u)_{i-\frac{1}{2}}^{*} S_{i-\frac{1}{2}}\right]. \tag{79}$$

*7.2.3. Energy equation*

In the energy equation (17), the total energy is expanded as

$$(\rho E)_i^{n+1} = (\rho E)_i^{*} + (\rho e)_p^{*} p_i' + (\rho e)_T^{*} T_i', \tag{80}$$

where only the internal energy is corrected, being the acoustic part (see Eq. (28)). The total enthalpy flux is written as,

$$(\rho H u)_{i+\frac{1}{2}} = (\rho H)_i u_{i+\frac{1}{2}} = (\rho e + p)_i u_{i+\frac{1}{2}} + \tfrac{1}{2}(\rho u^2)_i u_{i+\frac{1}{2}}. \tag{81}$$

According to the identification of acoustic terms (see Eq. (29)), only the first velocity term is corrected,

$$(\rho H u)_{i+\frac{1}{2}}^{n+1} = (\rho e + p)_i^{*}\frac{(\rho u)_{i+\frac{1}{2}}^{*} + (\rho u)_{i+\frac{1}{2}}'}{\rho_{i+\frac{1}{2}}^{*}} + \frac{1}{2}\left(\rho u^2\right)_i^{*} u_{i+\frac{1}{2}}^{*} = (\rho H)_i^{*} u_{i+\frac{1}{2}}^{*} + h_i^{*}(\rho u)_{i+\frac{1}{2}}' \tag{82}$$

and the momentum correction is again replaced by (72). The heat flux $q_{i+\frac{1}{2}}$ is discretized centrally and temperature corrections are introduced to avoid a diffusive time step limit,

$$q_{i+\frac{1}{2}}^{n+1} = \left(\kappa\frac{\partial T}{\partial x}\right)_{i+\frac{1}{2}}^{n+1} = \kappa\frac{(T_{i+1}^{*} + T_{i+1}') - (T_i^{*} + T_i')}{\Delta x}. \tag{83}$$

Introducing these terms into (17) results in a second equation containing both pressure and temperature corrections,

$$G_{i,i-1}p_{i-1}' + G_{i,i}p_i' + G_{i,i+1}p_{i+1}' + J_{i,i-1}T_{i-1}' + J_{i,i}T_i' + J_{i,i+1}T_{i+1}' = SE_i, \tag{84}$$

with

$$G_{i,i-1} = -\tau\left(\tau + \rho_{i-1}^* D_{i-\frac{1}{2}}\right)\frac{S_{i-\frac{1}{2}}}{S_i}h_{i-1}^{*}, \tag{85}$$

$$G_{i,i} = (\rho e)_p^* + \tau\left(\tau + \rho_i^* D_{i+\frac{1}{2}}\right)\frac{S_{i+\frac{1}{2}}}{S_i}h_i^* + \tau\left(\tau + \rho_{i-1}^* D_{i-\frac{1}{2}}\right)\frac{S_{i-\frac{1}{2}}}{S_i}h_{i-1}^*, \tag{86}$$

$$G_{i,i+1} = -\tau\left(\tau + \rho_i^* D_{i+\frac{1}{2}}\right)\frac{S_{i+\frac{1}{2}}}{S_i}h_i^*, \tag{87}$$

$$J_{i,i-1} = -\tau\frac{S_{i-\frac{1}{2}}}{S_i}\frac{\kappa}{\Delta x}, \tag{88}$$

$$J_{i,i} = (\rho e)_T^* + \frac{\tau}{S_i}\frac{\kappa}{\Delta x}\left(S_{i+\frac{1}{2}} + S_{i-\frac{1}{2}}\right), \tag{89}$$

$$J_{i,i+1} = -\tau\frac{S_{i+\frac{1}{2}}}{S_i}\frac{\kappa}{\Delta x}. \tag{90}$$

$$\begin{aligned} SE_i = {} & \rho E_i^n - \rho E_i^* - \frac{\tau}{S_i}\left[(\rho H)_i^* u_{i+\frac{1}{2}}^* S_{i+\frac{1}{2}} - (\rho H)_{i-1}^* u_{i-\frac{1}{2}}^* S_{i-\frac{1}{2}}\right] \\ & + \frac{\tau}{S_i}\frac{\kappa}{\Delta x}\left[(T_{i+1}^* - T_i^*)S_{i+\frac{1}{2}} - (T_i^* - T_{i-1}^*)S_{i-\frac{1}{2}}\right]. \end{aligned} \tag{91}$$

### 7.3. Procedure

The two correction equations (75) and (84) can be written in system form,

$$\begin{bmatrix} A_{i,i-1} & 0 \\ G_{i,i-1} & J_{i,i-1} \end{bmatrix}\begin{bmatrix} p'_{i-1} \\ T'_{i-1} \end{bmatrix} + \begin{bmatrix} A_{i,i} & \rho_T^* \\ G_{i,i} & J_{i,i} \end{bmatrix}\begin{bmatrix} p'_i \\ T'_i \end{bmatrix} + \begin{bmatrix} A_{i,i+1} & 0 \\ G_{i,i+1} & J_{i,i+1} \end{bmatrix}\begin{bmatrix} p'_{i+1} \\ T'_{i+1} \end{bmatrix} = \begin{bmatrix} SC_i \\ SE_i \end{bmatrix}, \tag{92}$$

which is in fact a $(2N \times 2N)$-system when all nodes are considered. This system is solved for the pressure and temperature corrections. Because of the coupled solution of the continuity and energy equation, we refer to the method as *coupled pressure and temperature correction algorithm*.

Finally, we summarize the successive steps of the algorithm:

- Predictor step: $\rho^*$ is determined from the continuity equation and $(\rho u)^*$ from the momentum equation. These values, together with the old pressure value $p^k$, determine an intermediate state *;
- Corrector step: coupled solution of the corrector equations (84) and (75) for pressure and temperature corrections. The pressure and temperature are updated;
- The density is updated through the equation of state $\rho^{n+1} = \rho(p^{n+1}, T^{n+1})$;
- Momentum corrections in the nodes are calculated with (67). Momentum is updated. An alternative is to use the implicit momentum equation (65) with the updated values for the pressure;
- The velocity is calculated from the updated values for momentum and density;
- A next iteration step is taken.

### 7.4. Boundary conditions

For the test case of the one-dimensional nozzle flow (see Sections 9.1 and 9.2.1), the first node ($i = 1$) and the last node ($i = N$) coincide with, respectively, the inlet and the outlet. At the inlet face we define values for density $\rho_{\text{in}}$ and velocity $u_{\text{in}}$. At the outlet face we define the pressure $p_{\text{out}}$. We use the following equations at the boundaries:

*Inlet*

- Predictor: $\rho_1^* = \rho_{\text{in}},\ (\rho u)_1^* = \rho_{\text{in}} u_{\text{in}}$;
- First correction equation: $p_1' - p_2' = p_2^k - p_1^k$;
- Second correction equation: $\frac{p_1'}{\rho_{in}} - T_1' = 0$;
- Momentum correction: $(\rho u)_1' = 0$.

*Outlet*

- Predictor: consider a control volume of length $\Delta x/2$ at the outlet,

$$\text{continuity}: \quad \rho_N^* - \rho_N^n + \frac{2\tau}{S_N}\left[\rho_N^* u_N^k S_N - \rho_{N-1}^* u_{N-\frac{1}{2}}^k S_{N-\frac{1}{2}}\right] = 0, \tag{93}$$

$$\text{momentum}: (\rho u)_N^* - (\rho u)_N^n + \frac{2\tau}{S_N}\left[(\rho u)_N^* u_N^k S_N - (\rho u)_{N-1}^* u_{N-\frac{1}{2}}^k S_{N-\frac{1}{2}}\right] = -2\tau(p_{\text{out}} - p_{N-\frac{1}{2}}^k); \tag{94}$$

- First correction equation: $p_N' = 0$;
- Second correction equation: $T_N' - T_{N-1}' = T_{N-1}^* - T_N^*$;
- Momentum: $(\rho u)_N^{n+1} = \rho_N^* u_{N-1}^{n+1} = \rho_N^* \frac{(\rho u)_{N-1}^{n+1}}{\rho_{N-1}^*}$.

Remark that these very simple boundary conditions are in fact very reflective [23], and therefore can destroy the convergence rate in some cases. For example, for a nozzle flow with a throat Mach number of 0.1, length $L = 100\Delta x$ and a convective $\text{CFL}_u$ of 1, an acoustic wave needs about 10 time steps to reach the boundaries, where it is reflected. At lower Mach numbers, the acoustic wave passes the boundaries within one time step, so that they do not get the risk to be reflected.

For the test case of the two-dimensional thermally driven cavity (see Section 9.2.2), a vertex-centered arrangement is used. The velocity is zero at the walls. The temperature is given at the right and the left wall. The upper and lower wall are isolated (adiabatic). The boundary conditions are used as follows:

- Predictor $\rho$*: the continuity equation for a boundary control volume is written as for internal nodes, but without convective contribution from the node(s) at the boundary;
- Predictor $(\rho u)$*, $(\rho v)$*: $(\rho u)_i^* = 0$, $(\rho v)_i^* = 0$ for boundary nodes;
- First correction equation: the continuity equation for a boundary control volume is written as for internal nodes, but without convective contribution from the node(s) at the boundary. Pressure and temperature corrections are introduced as usual;
- Second correction equation: at the upper and lower wall, the energy equation is written as for internal nodes, but without convective and conductive contributions from the node(s) at the wall. Pressure and temperature corrections are introduced as usual. At the left and right wall, we use $T' = 0$.

### 7.5. The special case of a perfect gas

#### 7.5.1. Perfect gas, no heat transfer: pressure-correction algorithm

Consider the frequent case of a perfect gas flow without heat transfer. With $\kappa$ and $(\rho e)_T$ equal to zero, all coefficients $J$ in (84) vanish. Consequently, all temperature corrections disappear from the energy equation, which becomes a pure pressure-correction equation,

$$G_{i,i-1} p_{i-1}' + G_{i,i} p_i' + G_{i,i+1} p_{i+1}' = SE_i. \tag{95}$$

This corresponds with the analysis made in Section 5.1: for the special case of a perfect gas, in absence of heat transfer, the energy equation determines the pressure. Thus, no coupled solution with the continuity equation is needed anymore.

For this special case, the algorithm is therefore implemented as follows:

- Predictor values $\rho_i^*$ and $(\rho u)_i^*$ are determined from (59) and (60). The predictor value $\rho^*$ is taken as an update for the density, i.e. $\rho^{n+1} = \rho^*$. Together with the old pressure values $p^k$, an intermediate state * is determined;
- The system of pressure-correction equations (95) is solved. The pressure is updated;
- Momentum is updated from (67);
- The velocity is calculated from the updated values for momentum and density;
- The equation of state is used to update the temperature, $T^{n+1} = p^{n+1}/\rho^{n+1}$;
- A next iteration step is taken.

In fact, the first correction equation of (92) is not used in this algorithm, and the continuity equation is only used in the predictor step. Indeed, for this special case, the energy equation is purely pressure-determining (see Eq. (37)). The continuity equation also contains acoustic information (see Eq. (35)), but can be considered as passive. For this special case, the obtained method is essentially the same as the one presented in [11] and [12].

Thus, the most straightforward way is to determine the pressure corrections from the energy-based correction equation. However, this does not mean that other ways are forbidden. Indeed, one could decide to determine the pressure corrections from the continuity-based correction equation under a frozen temperature,

$$A_{i,i-1}p'_{i-1} + A_{i,i}p'_i + A_{i,i+1}p'_{i+1} = 0 + SC_i \quad (T'_i = 0). \tag{96}$$

The energy equation is then used as an equation for the temperature. This is only possible if an old density value is used in the energy equation. For a detailed description of the latter implementation, we refer to Appendix B.

Though possible, it is clear that this second solution procedure is not the most efficient: the 'passive' equation (96) is used to determine the pressure. Due to the approximation $T' = 0$ in (96), several iterations would be needed to solve the system (92). If only one iteration is done, an underrelaxation of the pressure and the temperature is needed to keep the computation stable, leading to a slowdown of the convergence rate. This is illustrated in Section 9.1.

*7.5.2. Perfect gas, with heat transfer: coupled pressure and temperature correction algorithm*

When heat conduction is present, one could calculate the conductive flux from temperature values $T^*$ available from the predictor step. The fluid still being a perfect gas, the same procedure as above (adiabatic perfect gas) could be adopted, with some extra (known) temperature terms added in the RHS of the pressure-correction equation. In this method, an acoustic CFL-limit is still avoided. However, due to the explicit treatment of the conductive terms, a diffusive Neumann-limit will occur. This is confirmed by the tests performed in Section 9.2.

On the other hand, the coupled pressure and temperature correction method of Section 7.3 avoids the diffusive limit. This corresponds with the analysis of Section 5.2: in presence of heat transfer, the energy and continuity equation determine together both pressure and temperature, even if a perfect gas is considered.

Finally this remark. One could also think of replacing the temperature in the heat flux by the perfect gas law, as

$$q(T)^{n+1} = -\kappa\left(\frac{\partial T}{\partial x}\right)^{n+1} = -\kappa\frac{\partial}{\partial x}\left(\frac{p^k + p'}{\rho^*}\right). \tag{97}$$

Thus, some extra terms are added in the LHS of the pressure-correction equation, but no coupled solution with the continuity equation is needed. However, tests showed that this procedure cannot remove the diffusive limit. This can be explained in the following way. In (97), it may seem that the temperature is treated implicitly, because of the introduction of the pressure correction. However, for the density a predictor value is used. If there is heat transfer, this predictor value $\rho^*$ cannot be considered as the updated value $\rho^{n+1}$, since the temperature influence has to be inserted. Therefore, density would also have to be corrected, leading again to a coupled solution with the continuity equation. This becomes also clear from Eq. (58), written as

$$(\rho e)_p\left(\frac{\partial p}{\partial t} + u\frac{\partial p}{\partial x}\right) + (\rho e + p)\frac{\partial u}{\partial x} = \frac{\partial}{\partial x}\left(\kappa\frac{\partial T}{\partial x}\right) = \frac{\partial}{\partial x}\left[\kappa\left(T_p\frac{\partial p}{\partial x} + T_\rho\frac{\partial \rho}{\partial x}\right)\right] = \frac{\partial}{\partial x}\left[\kappa\left(\frac{1}{\rho}\frac{\partial p}{\partial x} - \frac{p}{\rho^2}\frac{\partial \rho}{\partial x}\right)\right], \tag{98}$$

where both terms in the RHS have to be treated implicitly to avoid a diffusive limit. When (97) is applied, however, only the pressure term is treated implicitly. The explicit treatment of the density term explains why a diffusive limit occurs.

## 8. Coupled pressure and temperature correction: in between the fully coupled and the fully segregated approach

The presented algorithm, referred to as *coupled pressure and temperature correction algorithm*, is situated in between the fully coupled and the fully segregated approach. The essential idea, is that the convective phenomenon (predictor step, momentum equation) is separated from the acoustic/thermodynamic phenomenon (corrector step, energy + continuity equation). We now present how this algorithm relates to other methods available in the literature.

### 8.1. Fully coupled approach

Writing the acoustic and diffusive terms implicitly, one can still decide to solve the system of equations in a coupled way. An example of such a semi-implicit method can be found in [20]. The underlying idea is the same as in our method, but the solution technique is different.

### 8.2. Fully segregated approach

This approach is adopted in a pressure-correction method, where the equations are fulfilled iteratively. In the literature, we distinguish two classes, based on how the pressure-correction equation is constructed. In the first class, the pressure-correction equation is derived from the continuity equation, in the second class, the energy equation is used for this purpose.

#### 8.2.1. Class 1: pressure-correction equation based on the continuity equation

Several examples of compressible pressure-correction methods exist, where the pressure-correction equation is derived from the continuity equation [5–10,16]. According to the foregoing analysis, this is not the most optimal way to determine the pressure corrections. The idea of using the continuity equation comes from the classical pressure-correction method, originally developed for constant density flows [4]. For that case, the continuity equation reduces to the kinematic constraint $\nabla \cdot \vec{v} = 0$, and the pressure-correction equation is derived from it. This is the right approach according to our analysis of Section 5.1 (special

case 1). Also for the case of a barotropic fluid, deriving the pressure-correction equation from the continuity equation is the preferred approach (Section 5.1, special case 2). An example can be found in [25] or [1].

*8.2.2. Class 2: pressure-correction equation based on the energy equation*

For a perfect gas flow without heat transfer, the pressure-corrections are determined most efficiently through the energy equation. In [23,24,26,27], a low Mach number perturbation analysis is used to show that for $M \to 0$ the energy equation reduces to the kinematic constraint $\nabla \cdot \vec{v} = 0$. The presented algorithms are based on that analysis, and are therefore only applicable in low Mach number flows. In [13], a non-conservative form of the equations is used. The algorithms in [11,12,14] are Mach-uniform, but no heat transfer is considered there.

## 9. Results

Though the algorithm was developed for a general fluid, so far only test cases with a perfect gas law were considered. For the adiabatic flow simulations, the fully segregated algorithm with a pressure-correction equation based on the energy equation was used.

### *9.1. Adiabatic flow*

First the Euler equations are considered, i.e., heat conduction and viscosity are neglected. As a test case, we take a converging–diverging one-dimensional nozzle. The section of the nozzle varies as

$$S(x) = \begin{cases} S_0, & 0 \leqslant x \leqslant \frac{2L}{28}, \\ S_0\left\{0.9 + 0.1\left[2\left(\frac{x-\frac{11L}{28}}{\frac{9L}{28}}\right)^2 - \left(\frac{x-\frac{11L}{28}}{\frac{9L}{28}}\right)^4\right]\right\}, & \frac{2L}{28} \leqslant x \leqslant \frac{20L}{28}, \\ S_0, & \frac{20L}{28} \leqslant x \leqslant L, \end{cases}$$

where $L$ is the length of the nozzle, $L = 1$ m. At the inlet boundary, the density and velocity are imposed. The pressure is fixed at the outlet boundary. The number of grid points is $N = 100$. The cell dimension is taken as reference length, $L_r = L/(N-1)$, so that $\Delta x = 1$. The other reference values are taken at atmospheric conditions, $T_r = 293$ K, $p_r = 101{,}300$ Pa. Both low and high speed flows are considered.

*9.1.1. Low speed*

We consider a subsonic nozzle flow with a throat Mach number $M_t$ of $10^{-3}$. The time step $\tau = \Delta t/\Delta x$ is calculated from a chosen convective CFL-number $\mathrm{CFL}_u$, i.e.

$$\tau = \frac{\mathrm{CFL}_u}{\max_i(u)}. \tag{99}$$

We remark that this corresponds with an acoustic CFL number, that is about 1000 times higher. Indeed,

$$\mathrm{CFL}_{u+c} = \tau \max_i(u+c) = \frac{\mathrm{CFL}_u}{\max_i(u)} \max_i(u+c) = \left(1 + \frac{1}{M_t}\right)\mathrm{CFL}_u \approx 1000\mathrm{CFL}_u. \tag{100}$$

First, we do the calculation with the fully segregated algorithm with an energy-based pressure-correction equation (Section 7.5). The convective $\mathrm{CFL}_u$ number was taken unity: there is no acoustic CFL limit. Fig. 1 shows the results for the Mach number and the pressure. Because the pressure variations are very small, we show a relative value, i.e., $\Delta p = p - p_{\mathrm{out}}$.

Fig. 2 shows the convergence plot. The vertical axis has a logarithmic scale and *Res Cont*, *Res Mom* and *Res Energ* represent the residual vectors of, respectively, the continuity, momentum and energy equation, of which the L2-norm is taken.

Next, we did the same calculation with the algorithm where pressure corrections are derived from the continuity equation (Section 7.5 and Appendix B). The computation could also be done at a $\mathrm{CFL}_u = 1$, but it could only be made stable by applying an underrelaxation for the temperature and pressure, i.e.

$$T^{n+1} = \omega T^* + (1-\omega)T^k, \tag{101}$$

$$p = p^k + \omega p'. \tag{102}$$

An underrelaxation factor $\omega$ of 0.7 was used. As explained, the need for underrelaxation arises from the non-optimal way to obtain the pressure corrections. Fig. 2 shows that for the latter algorithm, the convergence to the steady state is about three times slower.

The effect of the CFL-number on the convergence rate is illustrated in Fig. 3. The computation at $\mathrm{CFL}_u = 10$ converges more rapidly in the first time steps. This is due to the faster detection of the boundary conditions. However, at $\mathrm{CFL}_u = 10$ it takes more time steps to reach the steady state. This can be explained by approximations that are made during the segregation procedure, for example in (67). The latter was used to do the update for the momentum.

Finally, we compare computations for different nozzle flows, with throat Mach numbers of $10^{-2}$, $10^{-3}$ and $10^{-5}$. Fig. 4 shows a Mach-uniform convergence rate for the energy-based pressure-correction algorithm. The different levels of the final residuals is due to the so-called *cancellation problem* [28].

We conclude that the Mach-uniform algorithm performs very well for this low speed flow, with regard to accuracy as well as efficiency.

### 9.1.2. High speed

To illustrate that the algorithm is Mach-uniform, we also do a computation of a high speed flow. We consider a transonic nozzle with a shock at position $15L/28$.

Fig. 5 shows the convergence plot for a computation at $\mathrm{CFL}_u = 1$ and 10. We remark that for this case $\mathrm{CFL}_u \approx \mathrm{CFL}_{u+c}$ since the flow speed $u$ takes values close to the speed of sound $c$. Compared to the low Mach calculations, the convergence rate slows down. The first reason, is the stiffness in the system of equations at the sonic point $M = 1$. Like for the low Mach stiffness at $M = 0$, an eigenvalue becomes zero if $u = c$. The stiffness problem at low Mach numbers was taken out through the construction of the algorithm.

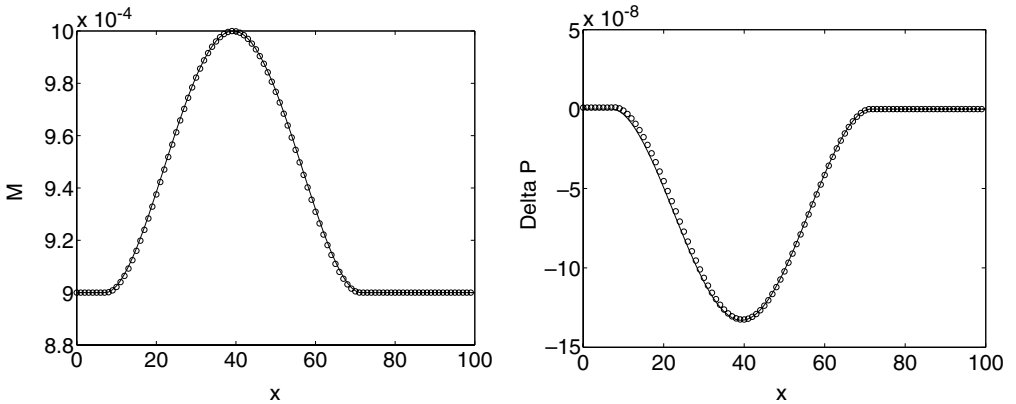


Fig. 1. Subsonic nozzle flow, $M_t = 0.001$. Mach number and relative pressure distribution. Symbols: Mach-uniform algorithm with pressure-correction equation based on the energy equation, $\mathrm{CFL}_u = 1$. Solid line: analytic solution.

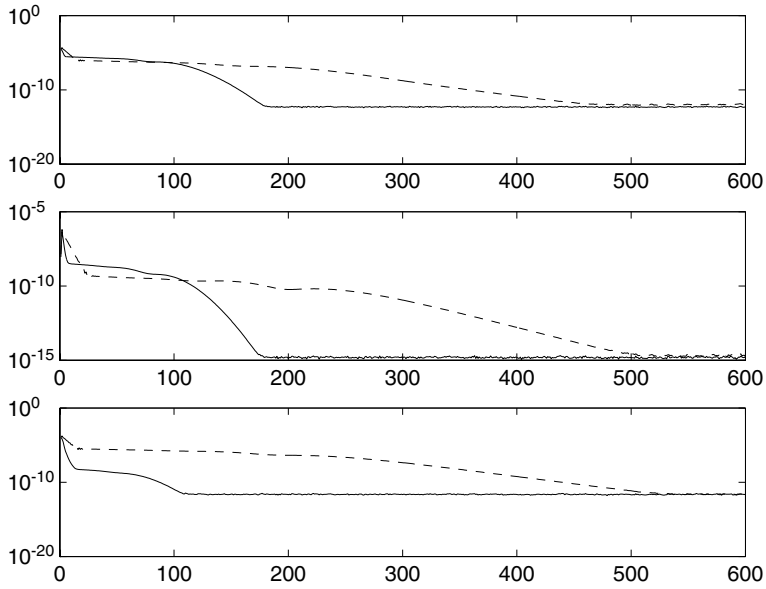


Fig. 2. Subsonic nozzle flow, $M_t = 0.001$. Res Cont, Res Im and Res Energ as a function of the number of time steps. $CFL_u = 1$. Solid line: Mach-uniform algorithm with pressure-correction equation based on the energy equation. Dashed line: algorithm based on the continuity equation (computation with underrelaxation (UR)).

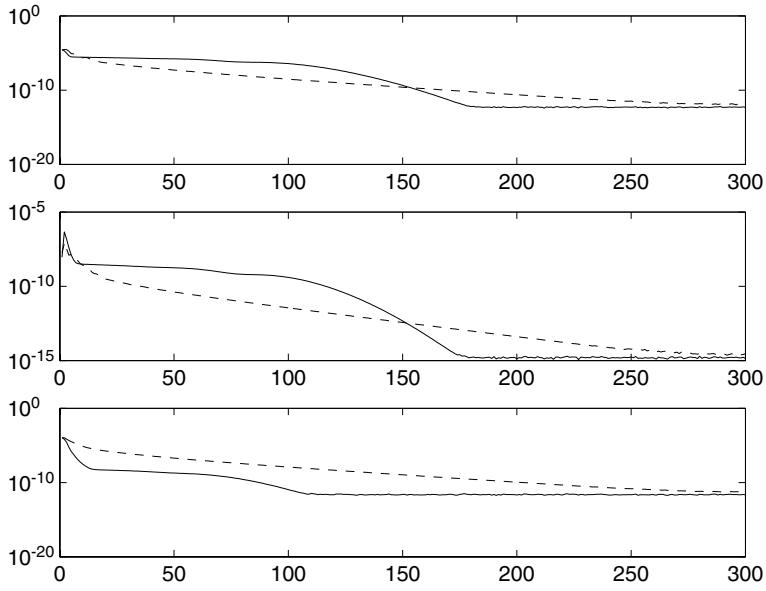


Fig. 3. Subsonic nozzle flow, $M_t = 0.001$. Res Cont, Res Im and Res Energ as a function of the number of time steps. Mach-uniform algorithm with pressure-correction equation based on the energy equation. Solid line: $CFL_u = 1$, dashed line: $CFL_u = 10$.

The second reason, is the higher sensitivity to the reflective boundary conditions (see Section 7.4). The Mach number and pressure distributions are shown in Fig. 6. The shock is somewhat smeared out because the upwind scheme is only first-order accurate.

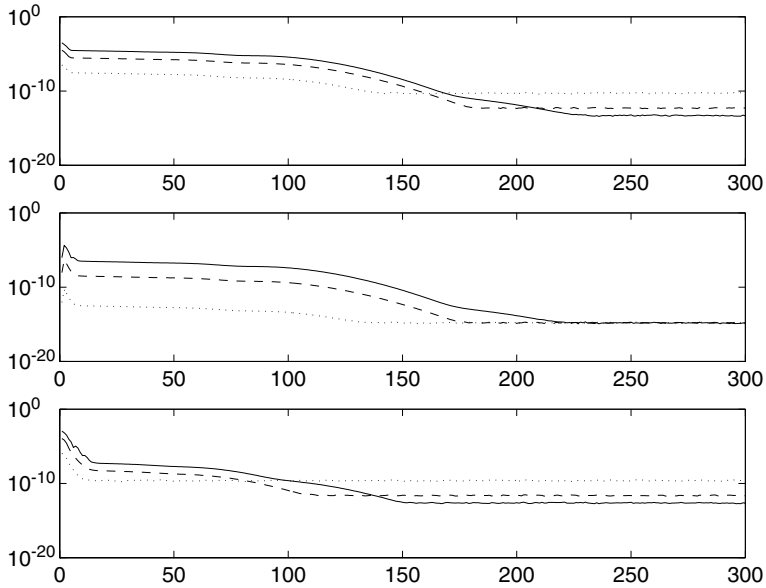


Fig. 4. Subsonic nozzle flows. Res Cont, Res Im and Res Energ as a function of the number of time steps. Mach-uniform algorithm with pressure-correction equation based on the energy equation, $\mathrm{CFL}_u = 1$. Solid line: $M_\mathrm{t} = 10^{-2}$, dashed line: $M_\mathrm{t} = 10^{-3}$, dotted line: $M_\mathrm{t} = 10^{-5}$.

We conclude that also for the high Mach numbers, we reach a good convergence rate and accuracy. Clearly, the algorithm shows Mach-uniform efficiency and accuracy.

### 9.2. Non-adiabatic flow

#### 9.2.1. One-dimensional nozzle flow

We consider again the test case of a one-dimensional nozzle flow, but now internal heat conduction is taken into account (friction is still neglected).

Just like for the adiabatic computations, no acoustic time step limit occurs. All the simulations are done at a convective $\mathrm{CFL}_u$ number of 1 at the throat.

If also a diffusive time step limit is to be avoided, the coupled solution of the energy and the continuity equation for both pressure and temperature corrections is needed. With the time step derived from the convective CFL number, (99), and $c = \sqrt{\gamma RT}/\hat{u}_\mathrm{r} = \sqrt{\gamma}$, the Von Neumann number is calculated as

$$Ne = \frac{\hat{\kappa}}{\hat{\rho}\hat{c}_p}\frac{\Delta\hat{t}}{\Delta\hat{x}^2} = \frac{\gamma-1}{\gamma}\frac{\kappa}{\rho}\frac{\Delta t}{\Delta x^2} = \frac{\gamma-1}{\gamma}\frac{\kappa}{\rho}\frac{\mathrm{CFL}_u}{u^{\max}\Delta x} = \frac{\gamma-1}{\gamma}\frac{\kappa}{\rho}\frac{\mathrm{CFL}_u}{\sqrt{\gamma}M_\mathrm{t}\Delta x}, \tag{103}$$

with $\rho \approx 1$, $\Delta x = 1$, $\mathrm{CFL}_u = 1$ and for the transonic case $M_\mathrm{t} \approx 1$. A realistic value for the non-dimensional heat conduction coefficient $\kappa$ can be derived from (12). For example, with

$$\hat{\kappa} = 0.0242\ \mathrm{W/(mK)(air)}, \tag{104}$$

$$\hat{p}_\mathrm{r} = 101,300\ \mathrm{Pa}, \tag{105}$$

$$\hat{T}_\mathrm{r} = 293\ \mathrm{K}, \tag{106}$$

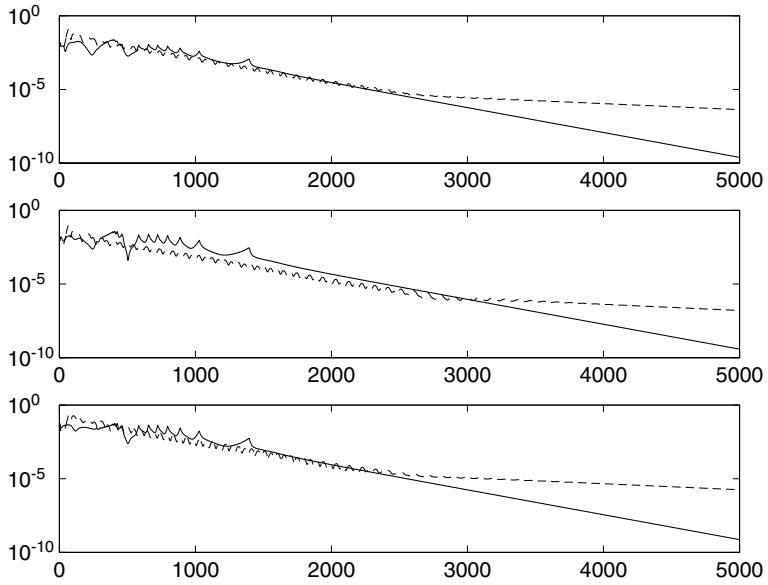


Fig. 5. Transonic nozzle flow. Res Cont, Res Im and Res Energ as a function of the number of time steps. Mach-uniform algorithm with pressure-correction equation based on the energy equation. Solid line: $CFL_u = 1$, dashed line: $CFL_u = 10$.

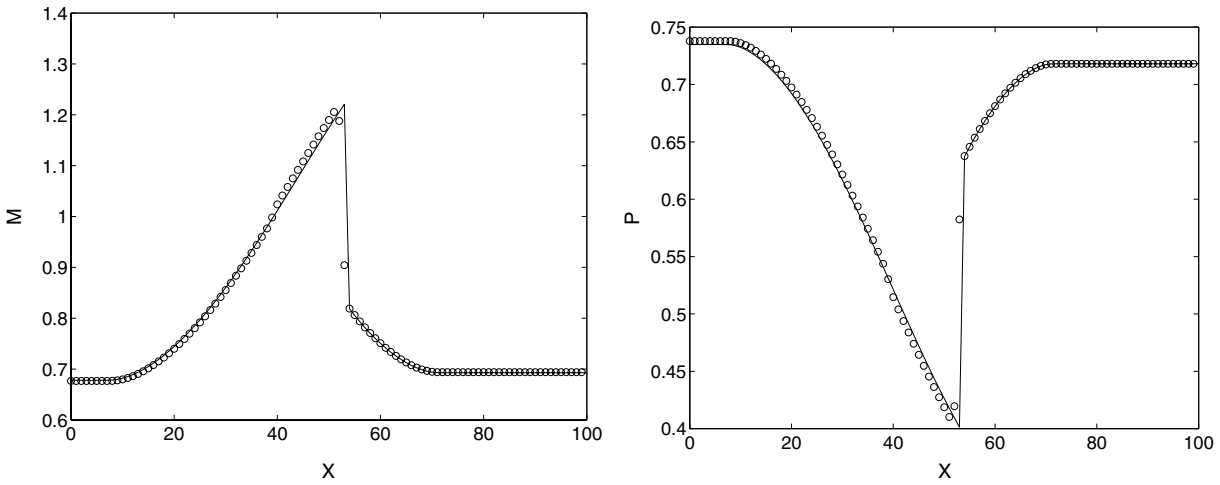


Fig. 6. Transonic nozzle flow. Mach number and pressure distribution. Symbols: Mach-uniform algorithm with pressure-correction equation based on the energy equation. $CFL_u = 1$. Solid line: analytic solution.

$$\hat{u}_r = \sqrt{R\hat{T}_r} = \sqrt{287.293}\ \mathrm{m/s}, \tag{107}$$

$$\hat{L}_r = \Delta\hat{x} = \hat{L}/N = 1\ \mathrm{m}/100, \tag{108}$$

we obtain $\kappa = 2.41 \times 10^{-5}$.

Table 1 shows the stability results for both the subsonic nozzle (throat Mach number $M_t = 0.01$ and 0.1) and transonic nozzle flow. The columns indicated with *exp* refer to an explicit calculation of the heat flux, which is added as extra term in the RHS of the pressure-correction equation based on the energy equation. *Coup* refers to the coupled pressure and temperature correction method. Different values for $\kappa$ were tested. We remark that $\kappa$ was risen above realistic values, but we mean to examine the presence of a diffusive limit. Table 1 also gives the number of time steps until convergence (residual $10^{-12}$ for the subsonic flow and $10^{-8}$ for the transonic flow), together with the time needed to do the calculation (just meant to compare the two algorithms). The results show clearly that the method with explicit heat flux becomes unstable as soon as the Von Neumann number becomes higher than order unity. The coupled method, however, stays stable no matter how high $\kappa$ is taken. Because the coupled method has to solve a $(2N \times 2N)$-system, versus only $(N \times N)$-systems in the explicit method, the calculation time to perform a certain number of time steps is longer with the coupled method. Remark that for the tests at $M_t = 0.1$ the convergence is much slower than for the calculations at lower Mach numbers. This is purely an effect of the used boundary conditions, which are reflective (see Section 7.4).

### 9.2.2. Thermally driven cavity

As a second test case for non-adiabatic flow, the two-dimensional thermally driven cavity problem is considered [26]. It concerns a squared cavity of dimension $L \times L$ filled with a perfect gas. The upper and lower walls are isolated (adiabatic). The left-hand side is heated (temperature $T_h$) and the right-hand side is cooled (temperature $T_c$), which causes a very slow circular movement of the gas due to natural convection. Besides heat conduction, also viscosity and gravity are taken into account, so the full Navier–Stokes equations are used.

This is a very challenging problem for our algorithm. Indeed, due to the very low Mach numbers ($M = O(10^{-7})$ for the case considered), no acoustic CFL-limit is allowed, since it would destroy the efficiency. Furthermore, in wall vicinity, the convective speeds are very small and the conduction becomes the dominating phenomenon. Therefore, also a diffusive Von Neumann-limit has to be avoided, so a coupled solution of the continuity and the energy equation is needed. Slightly different from the procedure in

Table 1
Nozzle flow

| Nozzle | $\kappa$ | *Ne* | Stable? | | Time steps | | Calc. time (in s) | |
|---|---|---|---|---|---|---|---|---|
| | | | Exp. | Coup. | Exp. | Coup. | Exp. | Coup. |
| Subsonic | $10^{-5}$ | $2.42 \times 10^{-4}$ | Yes | Yes | 220 | 208 | 19.6 | 23.5 |
| $M_t = 0.01$ | 0.01 | 0.242 | Yes | Yes | 259 | 224 | 22.3 | 24.5 |
| $Ne \approx \kappa \frac{0.242}{0.01}$ | 0.1 | 2.42 | No | Yes | – | 337 | – | 36.8 |
| | 1 | 24.2 | No | Yes | – | 646 | – | 70.4 |
| | 10 | 242 | No | Yes | – | 222 | – | 24.5 |
| Subsonic | $10^{-5}$ | $2.42 \times 10^{-5}$ | Yes | Yes | 1186 | 1180 | 101.2 | 128.8 |
| $M_t = 0.1$ | 0.1 | 0.242 | Yes | Yes | 1182 | 1176 | 101.1 | 128.4 |
| $Ne \approx \kappa \frac{0.242}{0.1}$ | 1 | 2.4 | No | Yes | – | 1211 | – | 132.2 |
| | 10 | 24.2 | No | Yes | – | 2019 | – | 228.7 |
| Transonic | $10^{-5}$ | $2.42 \times 10^{-6}$ | Yes | Yes | 3280 | 3309 | 290.0 | 372.9 |
| $Ne \approx \kappa \frac{0.242}{1}$ | 1 | 0.242 | Yes | Yes | 3169 | 3200 | 279.9 | 359.0 |
| | 10 | 2.42 | No | Yes | – | 4850 | – | 549.7 |
| | 100 | 24.2 | No | Yes | – | 3696 | – | 413.3 |

Stability, number of time steps until convergence and calculation time, for different values of $\kappa$. *Exp.*, pressure-correction equation based on the energy equation, heat flux calculated with $T^*$. *Coup.*, coupled pressure and temperature correction method.

Section 7.3, the final update of $(\rho u)$ is done by using the full momentum equations with updated pressure values, instead of using the approximation (67).

Also a diffusive limit due to the viscous terms is unwanted. Therefore, the viscous terms in the momentum equations are treated implicitly in the predictor step. They are discretized centrally and viscous velocity terms are written as $(\rho u)^*/\rho^*$ and $(\rho v)^*/\rho^*$. Remark that these linear terms are easier to treat than the non-linear convective terms. For the latter terms, linearizations and approximations due to the segregation procedure have to be adopted.

All technical details concerning this test case can be found in [29] or [30]. The dynamic viscosity $\mu = \mu(T)$ is given by Sutherland's law,

$$\mu(T) = \mu^s \left(\frac{T}{T^s}\right)^{3/2} \frac{T^s + S}{T + S}, \tag{109}$$

with $T^s = 273$ K, $S = 110.5$ K, $\mu^s = 1.68 \times 10^{-5}$ Pa s. The Prandl number $Pr$ is assumed to remain constant, equal to 0.71. The heat conduction coefficient is calculated as $\kappa(T) = \mu(T)c_p/Pr$. The heat transfer through the wall is represented by local and average Nusselt numbers $Nu$ and $\overline{Nu}$,

$$Nu(y) = \frac{L}{\kappa(T_r)(T_h - T_c)} \kappa \left.\frac{\partial T}{\partial x}\right|_{\text{wall}}, \tag{110}$$

$$\overline{Nu} = \frac{1}{L} \int_{y=0}^{y=L} Nu(y)\, \mathrm{d}y. \tag{111}$$

During the computation, the mean pressure level is adjusted in order to keep the mass content constant. A reduced pressure was used, i.e., the pressure subtracted with an offset value and the hydrostatic pressure field. The pressure dissipation terms to realise pressure–velocity coupling are introduced as in [30]. The gravity terms are calculated with starred predictor values for the density.

In [29], an extensive description of some benchmark solutions is given. We consider the case of a Rayleigh number $Ra = 10^3$ and a non-dimensional temperature difference $\epsilon = (T_h - T_c)/(2T_r) = 0.6$. Chosen reference values are $\hat{p}_r = 101,325$ Pa, $\hat{T}_r = 600$ K and $\hat{L}_r = L = 1$ m. Results are computed on a $129 \times 129$ stretched grid, of which the maximum aspect ratio is 80. A vertex-centered arrangement is used. A direct solver with LU-decomposition was used to solve the systems, though more efficient solvers will be considered in the future. The non-dimensional time step was taken $10^4$, which was about the highest value to keep the computation stable. It corresponds with a dimensional value

$$\Delta\hat{t} = \Delta t\, \hat{t}_r = \Delta t \frac{\hat{L}_r}{\sqrt{R\hat{T}_r}} \approx 24.1 \text{ s}. \tag{112}$$

Streamline patterns and temperature contours obtained after 1000 time steps are shown in Fig. 7. A convergence plot is given in Fig. 8. Values obtained for the mean Nusselt numbers and mean pressure are presented in Table 2.

Rounded at two significant digits, correct values are obtained. More correct digits would be obtained by a higher order discretization (only first order was used so far). This can be done without difficulties. However, the focus of this paper lies in the removal of the acoustic and diffusive time step limits. Therefore, we calculate the acoustic CFL number and the Von Neumann number. We calculate them at the left wall, where the highest temperature occurs, $\hat{T} \approx \hat{T}_h = (1 + \epsilon)\hat{T}_r = 960$ K. The left cells have an aspect ratio $\Delta y/\Delta x = 80$ and $\Delta\hat{x} \approx 0.0004$ m. With $u \ll c$ and $\Delta x \ll \Delta y$, we get for the maximum acoustic CFL-number

$$\mathrm{CFL}_{u+c} \approx \frac{\hat{c}\Delta\hat{t}}{\Delta\hat{x}} \approx \frac{\sqrt{\gamma R\hat{T}_h}\Delta\hat{t}}{\Delta\hat{x}} \approx 4\text{x}10^7, \tag{113}$$

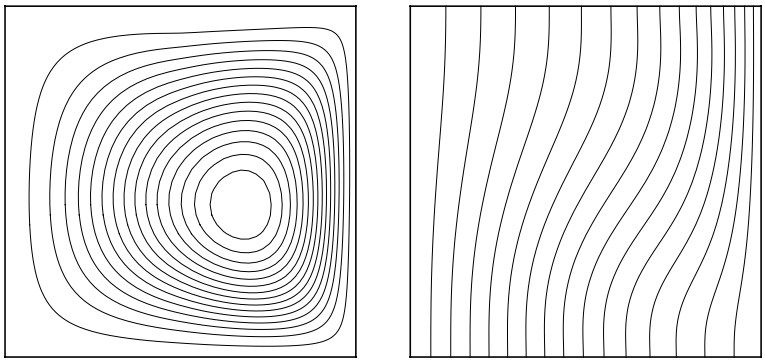

Fig. 7. Thermally driven cavity, $Ra = 1E3$, $\epsilon = 0.6$. Streamline patterns and temperature contours obtained with the coupled pressure and temperature correction method.

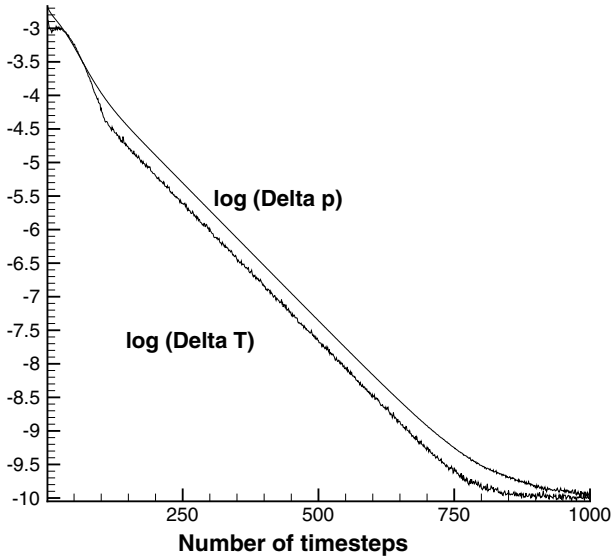


Fig. 8. Thermally driven cavity, $Ra = 1E3$, $\epsilon = 0.6$. Convergence plot: evolution of updates for pressure $|\Delta p| = |p^{n+1} - p^n|$ and temperature $|\Delta T| = |T^{n+1} - T^n|$. Mean value over all nodes. Logarithmic scale.

Table 2
Thermally driven cavity, $Ra = 1E3$, $\epsilon = 0.6$

| $Ra = 1E3$ $\epsilon = 0.6$ | Coupled pressure and temperature correction algorithm | Benchmark solution [29] |
|---|---|---|
| $\overline{Nu}_{\text{left}}$ | 1.1150 | 1.1077 |
| $\overline{Nu}_{\text{mid}}$ | 1.1116 | 1.1077 |
| $\overline{Nu}_{\text{right}}$ | 1.1149 | 1.1077 |
| $\bar{p}/p_{\text{r}}$ | 0.93973 | 0.93805 |

Values for the mean Nusselt numbers at the left wall, mid plane and right wall, and mean pressure.

which can be considered as infinity. We conclude that there is no stability limit coming from the acoustic terms. With

$$\hat{p} \approx \bar{p} = 0.94 \times 101,235 \text{ Pa} = 95245.5 \text{ Pa}, \tag{114}$$

$$\hat{\rho} \approx \hat{p}/(R\hat{T}_{\mathrm{h}}) \approx 0.346 \text{ kg/m}^3, \tag{115}$$

$$\hat{\mu}(\hat{T}_{\mathrm{h}}) \approx 3.969 \times 10^{-5} \text{ Pa s}, \tag{116}$$

$$\hat{\kappa}(\hat{T}_{\mathrm{h}}) \approx 0.0561 \text{ W/mK}, \tag{117}$$

$$\hat{\alpha} = \frac{\hat{\kappa}}{\hat{\rho}\hat{c}_p} \approx 1.617 \times 10^{-4} \text{ m}^2/\text{s}, \tag{118}$$

and $\Delta x \ll \Delta y$, we get for the maximum value of the Von Neumann number

$$Ne \approx \frac{\alpha \Delta t}{\Delta x^2} \approx 2 \times 10^4. \tag{119}$$

Clearly, there is no diffusive limit coming from the heat conduction terms. For the viscous terms, the same conclusion holds, as

$$Ne_{\mathrm{vis}} = \frac{\mu}{\rho} \frac{\Delta t}{\Delta x^2} \approx 2 \times 10^4. \tag{120}$$

## 10. Conclusion

We have presented a new type of algorithm: the coupled pressure- and temperature-correction algorithm. It finds its place in between the fully segregated pressure-correction algorithms and the fully coupled solution techniques. The essential idea is the separation of the convective phenomenon on the one side, and the acoustic/thermodynamic phenomenon on the other side. Based on a theoretical analysis, the algorithm was constructed so that Mach-uniform accuracy and efficiency are obtained, which was confirmed by the test results. Especially the removal of the acoustic and diffusive time step limits is an important feature. When the special case of a perfect gas without heat transfer is considered, the algorithm reduces to a fully segregated approach with a pressure-correction equation based on the energy equation. Finally, the easy extension toward general fluid applications, and the maintenance of time accuracy, are attractive aspects of this coupled pressure- and temperature-correction algorithm.

## Appendix A. The speed of sound expressed with a general equation of state

The isentropic speed of sound is defined as

$$c^2 = \left.\frac{\mathrm{d}p}{\mathrm{d}\rho}\right|_{s=\mathrm{cst}}. \tag{A.1}$$

With $\rho h = \rho e + p$, we have

$$\rho \, \mathrm{d}h + h \, \mathrm{d}\rho = \mathrm{d}(\rho e) + \mathrm{d}p. \tag{A.2}$$

For constant entropy, $T\mathrm{d}s = \mathrm{d}h - \mathrm{d}p/\rho = 0$, we get

$$h\,\mathrm{d}\rho = \mathrm{d}(\rho e) = (\rho e)_{\rho}^{p=\mathrm{cst}}\mathrm{d}\rho + (\rho e)_{p}^{\rho=\mathrm{cst}}\,\mathrm{d}p. \tag{A.3}$$

We obtain

$$c^2 = \frac{h - (\rho e)_{\rho}^{p=\mathrm{cst}}}{(\rho e)_{p}^{\rho=\mathrm{cst}}}, \tag{A.4}$$

with

$$(\rho e)_{\rho}^{p=\mathrm{cst}} = \left.\frac{\partial(\rho e)}{\partial\rho}\right|_{p=\mathrm{cst}} = \left(\left.\frac{\partial(\rho e)}{\partial T}\right|_{p=\mathrm{cst}}\right)\left(\left.\frac{\partial T}{\partial\rho}\right|_{p=\mathrm{cst}}\right) = \frac{(\rho e)_T}{\rho_T}, \tag{A.5}$$

$$(\rho e)_{p}^{\rho=\mathrm{cst}} = \left.\frac{\partial(\rho e)}{\partial p}\right|_{\rho=\mathrm{cst}}. \tag{A.6}$$

From

$$\mathrm{d}(\rho e) = (\rho e)_p\,\mathrm{d}p + (\rho e)_T\,\mathrm{d}T, \tag{A.7}$$

$$\mathrm{d}\rho = \rho_p\,\mathrm{d}p + \rho_T\,\mathrm{d}T = 0, \tag{A.8}$$

for constant $\rho$, we get

$$\mathrm{d}(\rho e) = (\rho e)_p\,\mathrm{d}p + (\rho e)_T\left(-\frac{\rho_p}{\rho_T}\,\mathrm{d}p\right), \tag{A.9}$$

$$\left.\frac{\partial(\rho e)}{\partial p}\right|_{\rho=\mathrm{cst}} = (\rho e)_p - \frac{\rho_p}{\rho_T}(\rho e)_T. \tag{A.10}$$

With (A.5) and (A.10), the speed of sound (A.4) becomes

$$c^2 = \frac{1}{\rho}\,\frac{(\rho e + p)\rho_T - \rho(\rho e)_T}{(\rho e)_p\rho_T - \rho_p(\rho e)_T}, \tag{A.11}$$

being valid for a general fluid. For a constant density fluid, $c$ becomes infinity. For a perfect gas, $\rho e = p/(\gamma - 1)$, we get the well-known expression,

$$c^2 = \frac{1}{\rho}\,\frac{(\rho e + p)}{(\rho e)_p} = \frac{\gamma p}{\rho}. \tag{A.12}$$

## Appendix B. Algorithm with pressure-correction equation based on the continuity equation

For the case of a perfect gas without heat transfer, an algorithm can be constructed where the pressure correction equation is derived from the continuity equation (see Section 7.5).

### *B.1. Predictor step*

A predictor step is taken from the momentum and the energy equation,

$$(\rho u)_i^* - (\rho u)_i^n + \frac{\tau}{S_i}\left[(\rho u)_i^* u_{i+\frac{1}{2}}^k S_{i+\frac{1}{2}} - (\rho u)_{i-1}^* u_{i-\frac{1}{2}}^k S_{i-\frac{1}{2}}\right] = -\tau(p_{i+\frac{1}{2}}^k - p_{i-\frac{1}{2}}^k), \tag{B.1}$$

$$(\rho E)_i^* - (\rho E)_i^n + \frac{\tau}{S_i}\left[(\rho E)_i^* u_{i+\frac{1}{2}}^k S_{i+\frac{1}{2}} - (\rho E)_{i-1}^* u_{i-\frac{1}{2}}^k S_{i-\frac{1}{2}}\right] = -\frac{\tau}{S_i}\left(p_{i+\frac{1}{2}}^k u_{i+\frac{1}{2}}^k S_{i+\frac{1}{2}} - p_{i-\frac{1}{2}}^k u_{i-\frac{1}{2}}^k S_{i-\frac{1}{2}}\right). \tag{B.2}$$

An intermediate state $u^*$, $T^*$, $p^k$ is determined by using an old density value, i.e.,

$$u_i^* = (\rho u)_i^*/\rho_i^k, \tag{B.3}$$

$$T_i^* = \frac{(\rho E)_i^*}{\rho_i^k} - \frac{1}{2}(u_i^*)^2. \tag{B.4}$$

### B.2. Corrector step

The relations between momentum corrections and pressure corrections are the same as in Section 7.2.1, namely

$$(\rho u)_i' = \frac{\tau}{S_i}\left\{(\rho u)_i^* D_{i+\frac{1}{2}}(p_{i+1}' - p_i')S_{i+\frac{1}{2}} - (\rho u)_{i-1}^* D_{i-\frac{1}{2}}(p_i' - p_{i-1}')S_{i-\frac{1}{2}}\right\} - \tau\left\{p_{i+\frac{1}{2}}' - p_{i-\frac{1}{2}}'\right\} \tag{B.5}$$

and

$$(\rho u)_{i+\frac{1}{2}}' = -\left[\tau + \rho_i^* D_{i+\frac{1}{2}}\right](p_{i+1}' - p_i'). \tag{B.6}$$

The pressure corrections are obtained from a continuity-based pressure-correction equation under a frozen temperature (see Eq. (96)),

$$A_{i,i-1}p_{i-1}' + A_{i,i}p_i' + A_{i,i+1}p_{i+1}' = SC_i. \tag{B.7}$$

### B.3. Procedure

The procedure is as follows:

- Predictor values $(\rho u)_i^*$ and $(\rho E)_i^*$ are determined from (B.1) and (B.2). Using old density values, an intermediate state $u^*$, $T^*$, $p^k$ is determined. The predictor value $T^*$ is used as an update for the temperature, $T^{n+1} = T^*$;
- The system of pressure-correction equations (B.7) is solved. The pressure is updated;
- Momentum is updated from (B.5);
- The equation of state is used to update the density, $\rho^{n+1} = p^{n+1}/T^{n+1}$;
- The velocity is calculated from the updated values of momentum and density;
- A next iteration step is taken.

## References

[1] P. Wesseling, D.R. van der Heul, C. Vuik, Unified methods for computing compressible and incompressible flows, in: Proceedings of ECCOMAS 2000, Barcelona, 11–14 september 2000.
[2] E. Turkel, Preconditioned methods for solving the incompressible and low speed compressible equations, Journal of Computational Physics 72 (2) (1987) 277–298.
[3] J.M. Weiss, W.A. Smith, Preconditioning applied to variable and constant density flows, AIAA Journal 33 (11) (1995) 2050–2057.
[4] S.V. Patankar, D.B. Spalding, A calculation procedure for heat, mass and momentum transfer in three-dimensional parabolic flows, International Journal of Heat and Mass Transfer 15 (1972) 1787–1806.

[5] I. Demirdžić, Ž. Lilek, M. Perić, A collocated finite volume method for predicting flows at all speeds, International Journal for Numerical Methods in Fluids 16 (1993) 1029–1050.
[6] P. Batten, F.S. Lien, M.A. Leschziner, A positivity-preserving pressure-correction method, Proceedings of the 15th International Conference on Numerical Methods in Fluid Dynamics, Lecture Notes in Physics, 490, Springer, 1996, pp. 148–151.
[7] W. Shyy, S.S. Thakur, H. Ouyang, J. Liu, E. Blosch, Numerical scheme for treating convection and pressure (chapter 2), Computational Techniques for Complex Transport Phenomena, Cambridge University Press, 1997, pp. 24–59.
[8] R.I. Issa, M.H. Javareshkian, Pressure-based compressible calculation method utilizing total variation diminishing schemes, AIAA Journal 36 (9) (1998) 1652–1657.
[9] H. Bijl, P. Wesseling, A unified method for computing incompressible and compressible flows in boundary-fitted coordinates, Journal of Computational Physics 141 (1998) 153–173.
[10] F. Moukalled, M. Darwish, A high-resolution pressure-based algorithm for fluid flow at all speeds, Journal of Computational Physics 168 (2001) 101–133.
[11] I. Wenneker, A. Segal, P. Wesseling, A Mach-uniform unstructured staggered grid method, International Journal for Numerical Methods in Fluids 40 (2002) 1209–1235.
[12] D.R. Van der Heul, C. Vuik, P. Wesseling, A conservative pressure correction method for flow at all speeds, Computers and Fluids 32 (2003) 1113–1132.
[13] V. Casulli, D. Greenspan, Pressure method for the numerical solution of transient, compressible fluid flows, International Journal for Numerical Methods in Fluids 4 (1984) 1001–1012.
[14] G. Patnaik, R.H. Guirguis, J.P. Boris, E.S. Oran, A barely implicit correction for flux-corrected transport, Journal of Computational Physics 71 (1987) 1–20.
[15] C.M. Rhie, W.L. Chow, Numerical study of the turbulent flow past an isolated airfoil with trailing edge separation, AIAA Journal 21 (11) (1982) 1525–1532.
[16] K. Nerinckx, J. Vierendeels, E. Dick, A Mach-uniform pressure correction algorithm using AUSM flux definitions, Advances in Fluid Mechanics V 40 (2004) 33–43.
[17] M.-S. Liou, C.J. Steffen, A new flux splitting scheme, Journal of Computational Physics 107 (1993) 23–39.
[18] M.-S. Liou, Mass flux schemes and connection to shock instability, Journal of Computational Physics 160 (2000) 623–648.
[19] J.R. Edwards, M.-S. Liou, Low-diffusion flux-splitting methods for flows at all speeds, AIAA Journal 36 (1998) 1610–1617.
[20] J. Vierendeels, K. Riemslagh, E. Dick, A multigrid semi-implicit line-method for viscous incompressible and low-Mach-number flows on high aspect ratio grids, Journal of Computational Physics 154 (1999) 310–341.
[21] S. Venkateswaran, L. Merkle, Analysis of preconditioning methods for the Euler and Navier–Stokes equations, VKI Lecture Series 1999-03 (1999).
[22] M. Perić, R. Kessler, G. Scheuerer, Comparison of finite-volume numerical methods with staggered and colocated grids, Computers & Fluids 16 (4) (1988) 389–403.
[23] B. Müller, Low Mach number asymptotics of the Navier–Stokes equations and numerical implications, VKI Lecture Series 1999-03 (1999).
[24] B. Müller, Low Mach number asymptotics of the Navier–Stokes equations, Journal of Engineering Mathematics 34 (1998) 97–109.
[25] D.R. van der Heul, C. Vuik, P. Wesseling, Efficient computation of flow with cavitation by compressible pressure correction, in: Proceedings of ECCOMAS 2000, Barcelona, 11–14 September 2000.
[26] D.R. Chenoweth, S. Paolucci, Natural convection in an enclosed vertical air layer with large horizontal temperature differences, Journal of Fluid Mechanics 169 (1986) 173–210.
[27] T. Schneider, N. Botta, K.J. Geratz, R. Klein, Extension of finite volume compressible flow solvers to multi-dimensional, variable density zero Mach number flows, Journal of Computational Physics 155 (1999) 248–286.
[28] J. Sesterhenn, B. Müller, H. Thomann, On the cancellation problem in calculating compressible low Mach number flows, Journal of Computational Physics 151 (1999) 597–615.
[29] J. Vierendeels, B. Merci, E. Dick, Benchmark solutions for the natural convective heat transfer problem in a square cavity with large horizontal temperature differences, International Journal of Numerical Methods for Heat and Fluid Flow 13 (8) (2003) 1057–1078.
[30] J. Vierendeels, B. Merci, E. Dick, A multigrid method for natural convective heat transfer with large temperature differences, Journal of Computational and Applied Mathematics 168 (2004) 509–517.